Interference and zero-bias anomaly in tunneling between Luttinger-liquid wires

Yaroslav Tserkovnyak and Bertrand I. Halperin
Lyman Laboratory of Physics, Harvard University, Cambridge, Massachusetts 02138, USA

Ophir M. Auslaender and Amir Yacoby
Department of Condensed Matter Physics, Weizmann Institute of Science, Rehovot 76100, Israel
(Received 13 February 2003; published 16 September 2003)

We present theoretical calculations and experimental measurements which reveal the Luttinger-liquid (LL) nature of elementary excitations in a system consisting of two quantum wires connected by a long narrow tunnel junction at the edge of a GaAs/AlGaAs bilayer heterostructure. The boundaries of the wires are important and lead to a characteristic interference pattern in measurements on short junctions. We show that the experimentally observed modulation of the conductance oscillation amplitude as a function of the voltage bias can be accounted for by spin-charge separation of the elementary excitations in the interacting wires. Furthermore, boundaries affect the LL exponents of the voltage and temperature dependence of the tunneling conductance at low energies. We show that the measured temperature dependence of the conductance zero-bias dip as well as the voltage modulation of the conductance oscillation pattern can be used to extract the electron interaction parameters in the wires.

DOI: 10.1103/PhysRevB.68.125312 PACS number(s): 73.21.Hb, 71.10.Pm, 73.23.Ad, 73.50.Jt

I. INTRODUCTION

Quasi-one-dimensional (1D) structures with gapless electronic excitations, such as carbon nanotubes, quantum Hall edge states, and confined states at the edge of a quantum-well heterostructure (i.e., quantum wires), possess unique properties which cannot be described by Landau's Fermi-liquid theory. Even small electron-electron interactions in a 1D confinement make inadequate the picture based on the existence of long-lived fermionic quasiparticles which can be mapped onto single-particle states in a free-electron gas. A powerful framework for understanding universal properties of 1D electron systems was put forward by the formulation of Luttinger-liquid (LL) theory.[1] (For a review see Ref. 2.) The spectral density, $\mathcal{A}(k,\omega)$, of the one-electron Green function in a Luttinger liquid is fundamentally different from that of a Fermi liquid: While the latter has one quasiparticle peak, the former has two singular peaks corresponding to the charge- and spin-density excitation modes.[3,4]

Tunnel-coupled quantum wires of high quality created at a cleaved edge of GaAs/AlGaAs double-quantum-well heterostructures appear to be an exceptional tool for probing spectral characteristics of a 1D system.[5–7] It is achieved[5] by measuring the differential conductance $G(V,B)$ as a function of the voltage bias between the wires, V, and magnetic field oriented perpendicular to the plane of the cleaved edge, B, allowing for simultaneous control of the energy and momentum of the tunneling electrons. In a recent paper[8] we demonstrated that the picture of noninteracting electrons can be used with great success to explain some of the most pronounced features of the conductance interference pattern arising from the finite size of the tunneling region. Taking electron-electron interactions into account was shown to explain experimentally observed long-period oscillation modulations in the V direction, which can be understood as a moiré pattern arising from spin-charge separation of electronic excitations. In this paper we use LL formalism to further investigate an interplay between electron correlations and the finite length of the tunnel junction, which allows us to understand peculiarities of the oscillations and the zero-bias anomaly in the measured tunneling conductance $G(V,B)$.

II. EXPERIMENTAL METHOD

In this section we describe the means by which we measure the tunneling conductance through a single isolated junction between two parallel wires.

A. Fabrication of the samples

The two parallel 1D wires are fabricated by cleaved-edge overgrowth (CEO), see Fig. 1 and Ref. 9. Initially, a GaAs/AlGaAs heterostructure with two closely situated parallel quantum wells is grown. The upper quantum well is 20-nm wide, the lower one is 30-nm wide, and they are separated by a 6-nm AlGaAs barrier about 300-meV high. We use a modulation doping sequence that renders only the upper quantum well occupied by a two-dimensional electron gas (2DEG) with a density $n \approx 2\times 10^{11}$ cm^{-2} and mobility $\mu \approx 3\times 10^{6}$ cm^2 V^{-1} s^{-1}. After cleaving the sample in the molecular-beam epitaxy growth chamber and growing a second modulation doping sequence, two parallel quantum wires are formed in the quantum wells along the whole edge of the sample. Both wires are tightly confined on three sides by atomically smooth planes and on the fourth side by the triangular potential formed at the cleaved edge.

Spanning across the sample are several tungsten top gates of width 2 μm that lie 2 μm from each other (two of these are depicted in Fig. 1). The differential conductance G of the wires is measured through indium contacts to the 2DEG straddling the top gates. While monitoring G with standard lock-in techniques (we use an excitation of 10 μV at 14 Hz) at $T=0.25$ K, we decrease the density of the electrons under

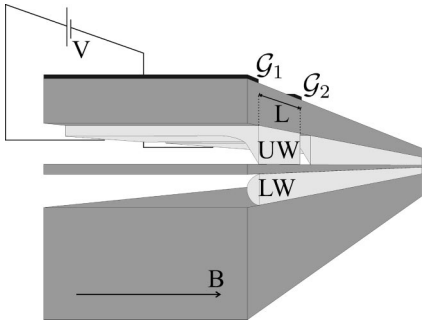

FIG. 1. Illustration of the sample and the contacting scheme. The sample is fabricated using the CEO method. The parallel 1D wires span along the whole cleaved edge (right facet in the schematic). The upper wire (UW) overlaps the two-dimensional electron gas (2DEG), while the lower wire (LW) is separated from them by a thin AlGaAs barrier (AlGaAs is dark gray in the schematic; electron liquids are light gray). Contacts to the wires are made through the 2DEG. Several tungsten top gates can be biased to deplete the electrons under them: We show only $\mathcal{G}_1$, here biased to deplete the 2DEG and both wires, and $\mathcal{G}_2$, here biased to deplete only the 2DEG and the upper wire. The magnetic field B is perpendicular to the plane defined by the wires. The depicted configuration allows the study of the conductance of a tunnel junction between a section of length L of the upper wire and a semi-infinite lower wire.

the gate by decreasing the voltage on it (V_g). At $V_g = V_{2D}$, the 2DEG depletes and G drops sharply, because the electrons have to scatter into the wires in order to pass under the gate. For $V_{2D} > V_g > V_U$ the conductance drops stepwise each time a mode in the upper wire is depleted.[10] In this voltage range, the contribution of the lower wire to G is negligible because it is separated from the upper quantum well by a tunnel barrier. When $V_g = V_U$, the upper wire depletes and only the lower wire can carry electrons under the gate. This last conduction channel finally depletes at V_L and G is suppressed to zero.

B. Measurement on an isolated tunnel junction

The measurements are performed in the configuration depicted in Fig. 1. The source is the 2DEG between two gates, $\mathcal{G}_1$ and $\mathcal{G}_2$ in Fig. 1, the voltages on which are $V_1 < V_L$ and $V_L < V_2 < V_U$, respectively. The upper wire between these gates is at electrochemical equilibrium with the source being the 2DEG. This side of the circuit is separated by the tunnel junction we wish to study from the drain. The drain is the 2DEG to the right of $\mathcal{G}_2$ (the semi-infinite 2DEG in Fig. 1) and it is in equilibrium with the right, semi-infinite, upper wire and with the whole, semi-infinite, lower wire in Fig. 1. Thus, any voltage difference (V) induced between the source and the drain drops on the narrow tunnel junction between the gates. This configuration gives us control over both the energy and the momentum of the tunneling electrons, as explained below. An additional gate lying between $\mathcal{G}_1$ and $\mathcal{G}_2$ (not shown in Fig. 1) allows us to deplete the 2DEG in the center of the source, thus reducing the screening of the interactions in the wires by the 2DEG.

The energy of the electrons tunneling between the wires is given by eV, $-e$ being the electron charge. The tunneling process occurs along the whole length L of the tunnel junction. Therefore, momentum is conserved to within an uncertainty of order $2\pi/L \ll k_F$, where k_F is a typical Fermi wave vector in the wires. We can shift the momentum of the tunneling electrons with a magnetic field (B) perpendicular to the plane defined by the wires. The value of the shift is $\hbar q_B = eBd$, where d is the center-to-center distance between the wires.

III. DESCRIPTION OF THE EXPERIMENTAL RESULTS

In the experiment we measure the nonlinear differential tunneling conductance $G(V,B)$ through a junction between two parallel wires. The sample on which we report here contains four top gates allowing us to vary the length of the junction L by choosing different combinations of gates. We have studied in detail junctions with $L = 2$, 4, 6, and 10 μm as well as symmetric junctions ($L = \infty$). The results presented here are from junctions with $L = 2$, 6, and 10 μm. Many of the effects that we measure rely on the smallness of $1/L$, while others (which we address here in detail) are present only when L is finite.

A. Dispersions of elementary excitations in the wires

By mapping out $G(V,B)$ we determine the dispersion curves of the wires.[5] These are given by the curves that are traced by the main peaks as seen in Fig. 2. We can understand their gross features employing a noninteracting electron picture:[5] The peaks result from tunneling between a Fermi point in one wire and a mode in the other wire. Since each occupied mode has two Fermi points, two copies of the dispersion show up in the $G(V,B)$ scan. All in all, for each pair of occupied modes in the two wires we expect to observe four dispersions, because there are four Fermi points involved: $\pm k^i_{Fu}$ and $\pm k^j_{Fl}$. (Indices i and j label various modes in the wires; u and l denote the upper and the lower wires.) In reality, we observe only some of the transitions: For example, by carefully studying Fig. 2 one can distinguish dispersions of three modes in the upper wire and five in the lower one, but only the following transitions seem to have a sizable signal: $|u_1\rangle \leftrightarrow |l_1\rangle$, $|u_3\rangle \leftrightarrow |l_2\rangle$, and $|u_2\rangle \leftrightarrow |l_{3,4,5}\rangle$, where the order in the list is of decreasing $B_2^{i,j}$ (see below); $|u_3\rangle$ is the 2DEG occupying the upper quantum well.[5] Such selection rules are related to the shape of the wave functions in the direction perpendicular to the cleaved edge. In identical wires, one would expect only the transitions $|u_n\rangle \leftrightarrow |l_n\rangle$ to appear, due to the orthogonality between different modes. In dissimilar wires, the selection rules are different and less strict, so other transitions are observed.

The dispersions allow us to extract the densities of electrons in each mode, $n^i_{u(l)} = (2/\pi) k^i_{Fu(l)}$, as follows. Tunneling among each pair of occupied modes is enhanced near $V = 0$ at two values of $B > 0$, where the two curves in $G(V,B)$ cross. In the first (in the following referred to as the ''lower crossing point''), which occurs at $B_1^{i,j}$, the direction in which the electrons propagate is conserved in the tunneling process. In the second (referred to as the ''upper crossing point''), the Lorentz force exerted by $B_2^{i,j}$ exactly compen-

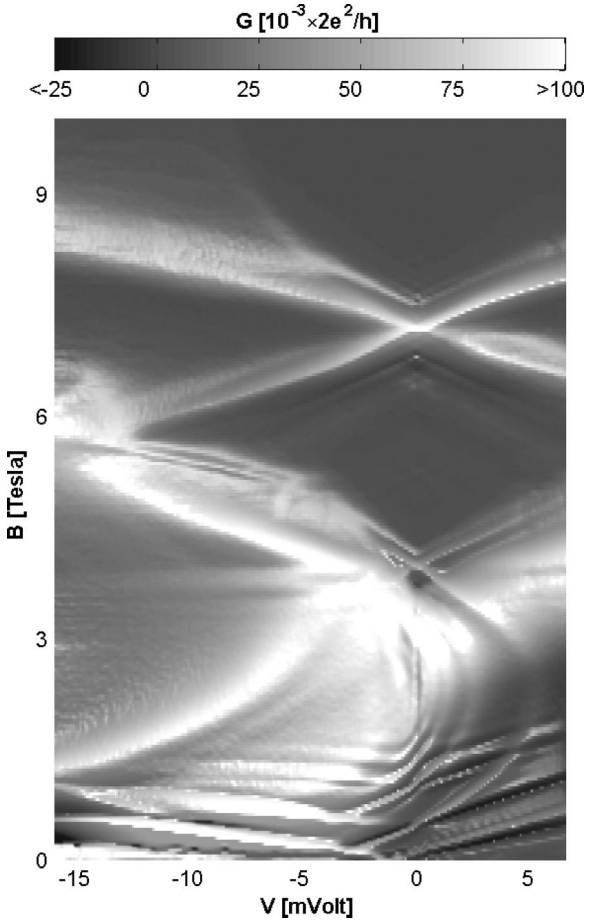

FIG. 2. Plot of $G(V,B)$ for a 10-μm junction. Higher values of the conductance are depicted in lighter shades: The top bar gives the key.

sates for the momentum mismatch between oppositely moving electrons, and the direction of propagation of the tunneling electrons reverses. In wires with a vanishing cross section, these crossing points occur at

$$|B^{i,j}_{1(2)}| = \frac{\hbar}{ed}|k^i_{\mathrm{Fu}} \mp k^j_{\mathrm{Fl}}|. \tag{1}$$

In principle, Eq. (1) can be used to extract the densities of the modes, regardless of electron-electron interactions in the wires[6] or mesoscopic charging[11] that can merely smear them at a finite voltage bias. In realistic wires that have a finite cross section, finding the densities is hampered by the weak magnetic-field dependence that they acquire. This difficulty is overcome by a simple fitting procedure that we have developed: We assume that all the modes in a wire have the same field dependence, a reasonable assumption for our tight-confining potential in the growth direction of the quantum wells. We then guess the $B=0$ occupations of the modes in each wire, $n^i_u(0)$ and $n^j_l(0)$, and calculate their field dependencies. If the resulting dispersions do not cross at $B^{i,j}_{1(2)}$, we adjust $n^i_u(0)$ and $n^j_l(0)$ and repeat the procedure. This is done iteratively for all the crossing points that we see, because changing the occupation of one mode affects the field dependence of all the other occupations in a wire. The dispersion that we use is that of noninteracting electrons in a finite quantum well, in the presence of an in-plane magnetic field. Such a dispersion depends only on the width and depth of the well and on the band mass of electrons in GaAs.

In every case we have studied, we see clear deviations of the measured dispersions from the calculated noninteracting ones at a finite bias. In particular, we find that the velocities of some excitations are enhanced relative to the Fermi velocities $v_{\mathrm{Fu(l)}}$. The former are given by

$$v_p = \frac{1}{d}\frac{\partial V}{\partial B}\bigg|_{B^{i,j}_{1(2)}} \tag{2}$$

(along the observed main peaks), while the latter can be obtained by the calculated slope of the (noninteracting) dispersions at the Fermi points. This velocity enhancement is thought to correspond to the charge-density modes and can be accounted for by electron-electron interactions in the wires.[6,5]

The ability to determine the dispersion relations relies on the high quality of the junctions to sustain momentum-conserving tunneling. Momentum relaxation ensues as soon as invariance to translations is broken. The most obvious mechanism by which this occurs is the finiteness of L. We find that we indeed observe its effects. The second mechanism is the disorder inherent to all semiconductor devices, some effects of which seem also to be observed.

B. Oscillations

The most spectacular manifestation of the breaking of translational invariance is the appearance of a regular pattern of oscillations away from the dispersion curves. Figures 3(a) and 4(a) are typical examples of the patterns that we measure at low magnetic field. In this range of field, the lines that correspond to the dispersion curves appear as the pronounced peaks that extend diagonally across the figures. In addition to these we observe numerous secondary peaks running parallel to the main dispersion curves. These sidelobes always appear to the right of the wire dispersions, in the region that corresponds to momentum-conserving tunneling for an upper wire with a reduced density. As a result, we see a checkerboard pattern of oscillations in region I, a hatched pattern in region II, and no regular pattern in region III [see Figs. 3(a) and 4(a) for the definitions].

The interference pattern also appears near the upper crossing point at high magnetic field. A typical example is shown in Fig. 5.

The frequency of the oscillations depends on L. When L is increased from 2 μm, Fig. 3, to 6 μm, Fig. 4, the frequency in bias (ΔV) and in field (ΔB) increases by a factor of about 3. The period is approximately related to the length of the junction through the formula

$$\Delta V L/v_{\mathrm{F}} = \Delta B L d = \phi_0, \tag{3}$$

where $\phi_0 = 2\pi\hbar/e$ is the quantum of flux.

A close examination of the low-field oscillations reveals

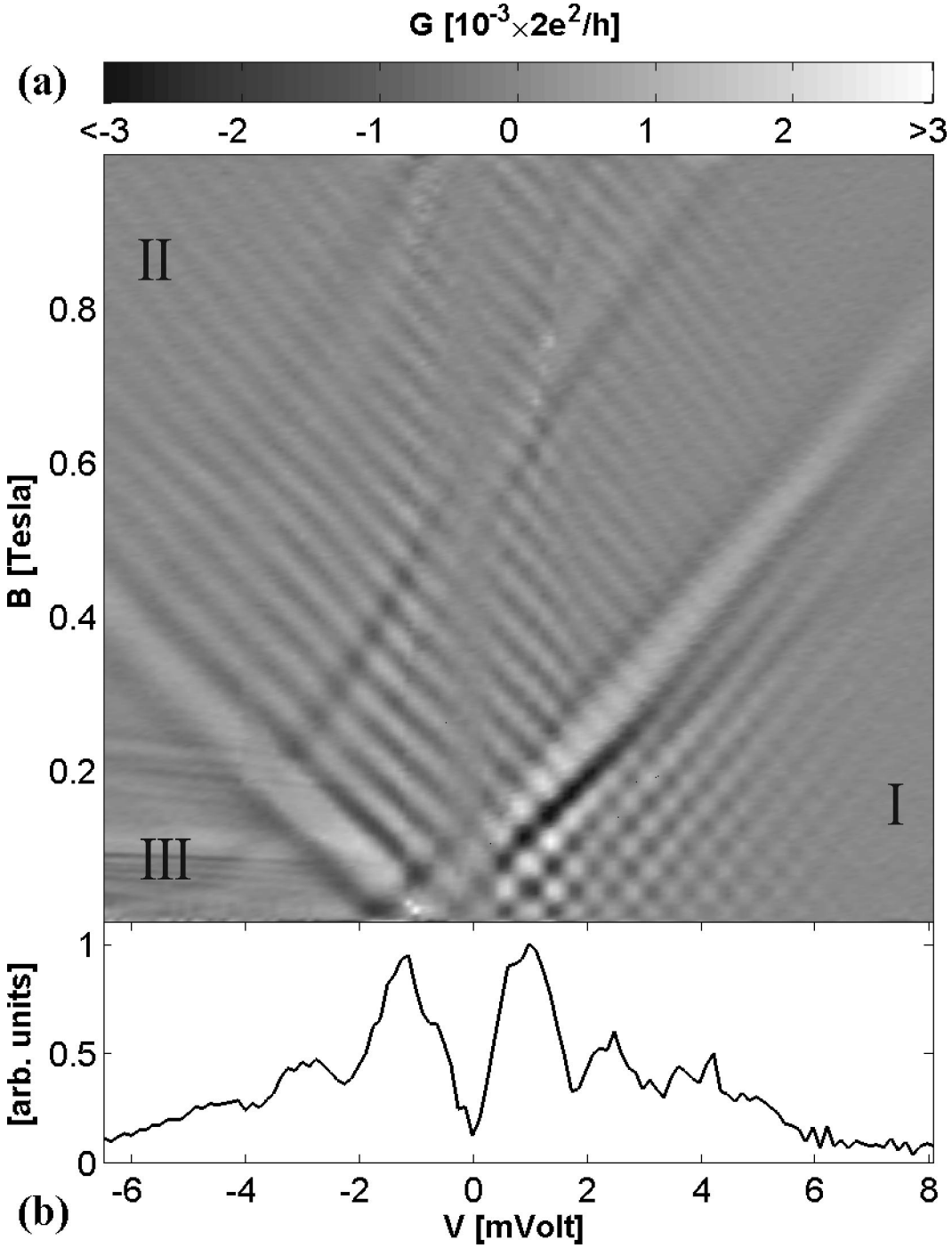

FIG. 3. Nonlinear conductance oscillations at low field from a 2-μm junction. (a) Oscillations as a function of both B and V. (A smoothed background has been subtracted to emphasize the oscillations.) The brightest (and darkest) lines, corresponding to tunneling between the lowest modes, break the V-B plain into regions I, II, and III. Additional positively-sloped bright and dark lines in II arise from other 1D channels in the wires and are disregarded in our theoretical analysis. Also present is a slow modulation of the strength of the oscillations along the abscissa. (b) Absolute value of the peak of the Fourier transform of $S^{1-1/\beta}G(V,S^{1+1/\beta})$ at fixed V in region II as a function of V. (See Sec. IV B 1 for the definition of S, β, and other details.) Its slow modulation as a function of V is easily discerned.

an interesting behavior of their envelope. Notable is the suppression of $G(V,B)$ near $V=0$ which is independent of field. Also visible are faint vertical gray stripes, where the amplitude of the oscillations in the B direction is reduced. The modulation of the oscillation amplitude, as a function of V, is shown in Figs. 3(b) and 4(b). The oscillatory part of G thus depends on V on two major scales: The faster scale (0.5 mV for $L=2$ μm) corresponds to the oscillations described by Eq. (3). The slower scale (2 mV for $L=2$ μm) governs the distance between the stripes of suppressed $G(V,B)$ parallel to the field axis, including the zero-bias suppression. Like the fast scale, the slow scale is roughly

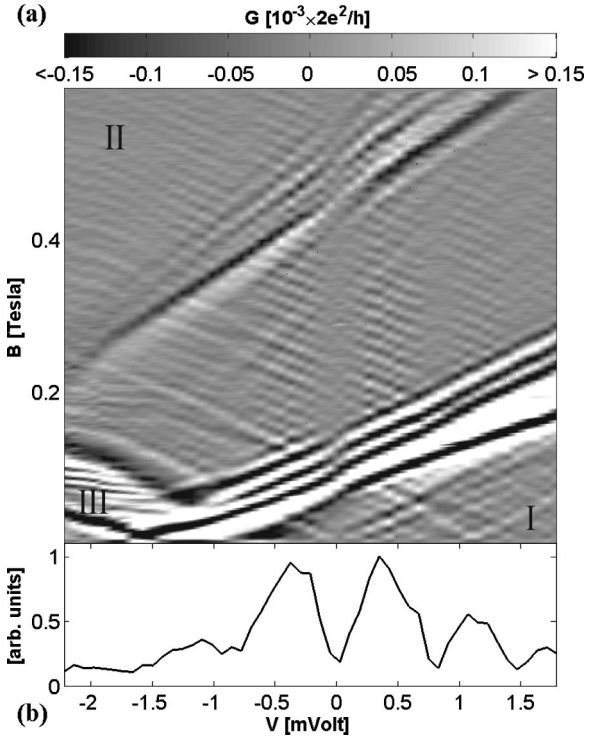

FIG. 4. Same as Fig. 3 but for a 6-μm junction. Note that the oscillations are approximately three times faster than in Fig. 3, as expected from Eq. (3). For this junction, there are several additional sidelobes present on the left of the principal peaks, unlike in the case of the shorter junction in Fig. 3.

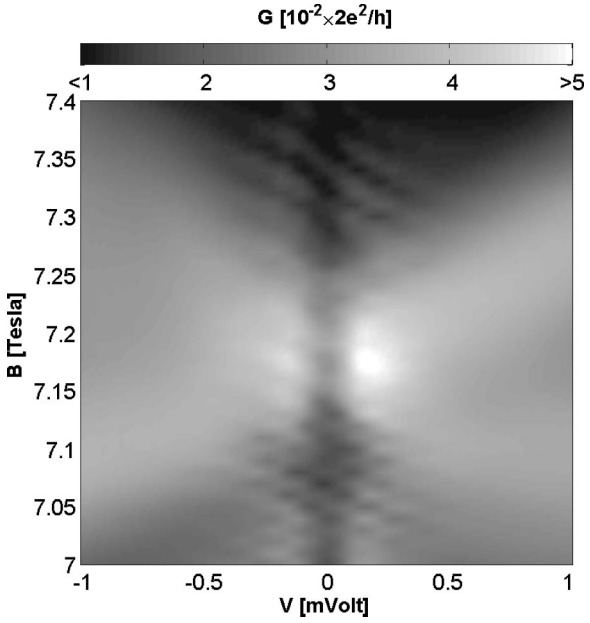

FIG. 5. $G(V,B)$ near the upper crossing point for a 6-μm junction. In this measurement, a central 2-μm gate midway between $\mathcal{G}_1$ and $\mathcal{G}_2$ is biased to deplete all upper-wire modes except the lowest one. One can see a pattern of oscillations around the dispersion peaks.

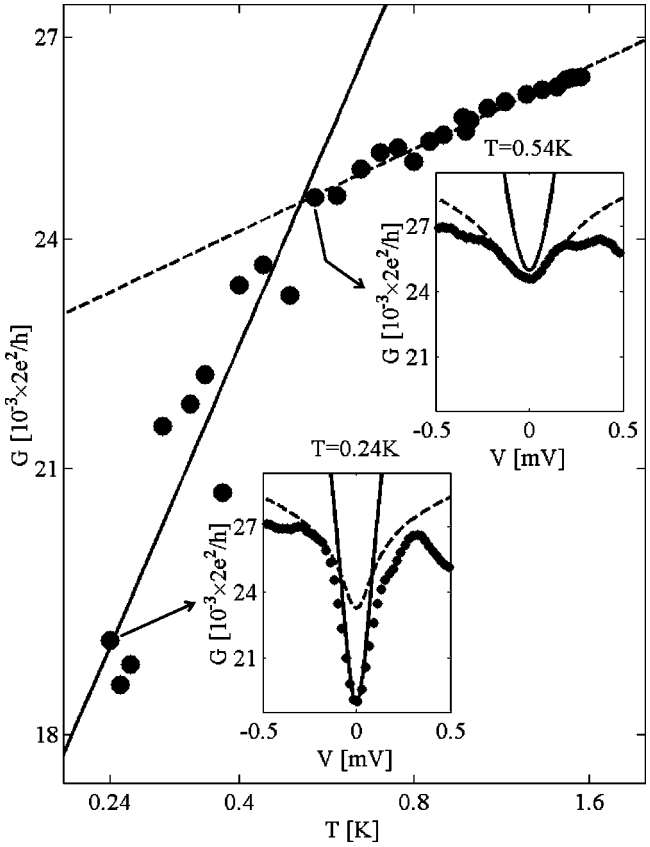

FIG. 6. Zero-voltage dip of the tunneling conductance G as a function of temperature on a log-log scale. The circles show measurements on a 6-μm junction at $B=2.5$ T; the lines are a fit using $G\propto T^{\alpha}$ for $V=0$. The dashed line is the result for $\alpha=\alpha_{\rm bulk}(g_l)=0.07$ while the solid line is the result for $\alpha=\alpha_{\rm end}(g_l)=0.35$, with $g_l=0.59$ (and $g_u=1$) in Eqs. (49) and (50), respectively; see Sec. IV C 2 for a discussion. Insets: $G(V)$ for $T=0.24$ K and $T=0.54$ K (the temperature dependence was generated from the $V=0$ point of such scans). The curves were calculated with Eq. (51) and using the above value of g_l extracted from the fit of the temperature dependence of the dip. [We obtained $F_{\alpha}(x)$ by convoluting the derivative of the Fermi distribution in the 2D leads, $[1/(4k_BT)]\mathrm{sech}^2[eV/(2k_BT)]$, with the finite-temperature tunneling density of states in the lower wire, see Eq. (5) in Ref. 12.] The dashed lines correspond to the $\alpha_{\rm bulk}$ value of the exponent while the solid lines to $\alpha_{\rm end}$.

inversely proportional to the lithographic length of the tunneling region.

C. A dip in the tunneling conductance

Prominent in all scans that have high enough resolution in V is a strong suppression of the conductance near $V=0$ at all magnetic fields. The width of this conductance dip is of order of 0.1 mV, see Figs. 2 and 5. The size of the dip is very sensitive to temperature, as depicted in Fig. 6, and it exists for $T\lesssim 1.0$ K.

IV. THEORY AND DISCUSSION

The 1D modes in the upper quantum well are coupled to the 2DEG via an elastic 1D-2D scattering which ensures a

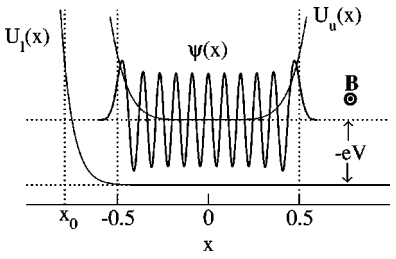

FIG. 7. Schematic picture of the theoretical model. The upper wire is formed by a potential well $U_u(x)$ created by gates $\mathcal{G}_1$ and $\mathcal{G}_2$ (shown in Fig. 1) and the lower wire is semi-infinite with the left boundary $U_l(x)$ at gate $\mathcal{G}_1$. $\psi(x)$ is an electron wave function in the upper wire. The energy and momentum of the tunneling electrons are governed by the voltage bias V and magnetic field B.

good electronic transfer between the extended and confined states of the well.[13] In addition to tunneling between the confined states in the wires, if the extended states have an appreciable weight at the edge, there will be a direct transition from the 2DEG to the lower wire. With this in mind, we separate the total current into two contributions, one due to tunneling between 1D bands and the other due to direct tunneling from the 2DEG. As explained in Sec. III A, each of the wires carries several 1D modes. In our analysis and comparison with the experiment, we will only consider the transition between the lowest 1D bands of the wires (i.e., the bands with the largest Fermi momentum), $|u_1\rangle \leftrightarrow |l_1\rangle$, and the direct tunneling from the 2DEG, $|u_3\rangle \leftrightarrow |l_2\rangle$, with both having a strong signal, as seen in Fig. 2. In each wire, the 1D modes interact with each other, but since the bands have very different Fermi velocities, we treat them independently. This is a reasonable approximation, as explained in Appendix A.

The geometry for our theoretical description is shown in Fig. 7. The potentials $U_u(x)$ and $U_l(x)$ are felt by electrons in the upper and lower quantum wires, respectively. The electrons in the upper wire are confined to a region of finite length by potential gates at both its ends (see the source region in Fig. 1). One of these gates ($\mathcal{G}_1$) causes the electrons in the lower wire to be reflected at one end, but the other ($\mathcal{G}_2$) allows them to pass freely under it. The effective tunneling region is determined by the length of the upper wire, which is approximately the region $|x|<L/2$ in Fig. 7. The magnetic field, B, gives a momentum boost $\hbar q_B = eBd$ along the x axis for the electrons tunneling from the upper to the lower wire.

First, we develop a general formalism in Sec. IV A. We then apply it to study the conductance interference pattern in Sec. IV B and the zero-bias anomaly regime in Sec. IV C.

A. General formalism

Let us first consider transport between two 1D bands in the wires. We use the following model Hamiltonian to study the intermode tunneling in the system:

$$H=\sum_{\nu=u,l} H_0^{\nu}+\sum_{\nu\nu'=u,l} H_{\rm int}^{\nu\nu'}+H_{\rm 1D\text{-}2D}+H_{\rm tun}. \qquad (4)$$

H_0^{ν} is the kinetic energy of the electrons [$\nu=u(l)$ labels the upper (lower) wire], $H_{\rm int}^{\nu\nu}$ [$H_{\rm int}^{ul}$] describes spin-independent electron-electron interactions in (between) the wires, $H_{\rm 1D\text{-}2D}$ is an effective Hamiltonian for the 1D-2D scattering of electrons in the top quantum well, and $H_{\rm tun}$ is the tunneling Hamiltonian:

$$H_0^{\nu}=v_{{\rm F}\nu}\sum_s \int dx[\Psi_{Rs\nu}^{\dagger}(-i\partial_x)\Psi_{Rs\nu}-\Psi_{Ls\nu}^{\dagger}(-i\partial_x)\Psi_{Ls\nu}], \qquad (5)$$

$$H_{\rm int}^{\nu\nu'}=\frac{1}{4\pi}\sum_{ss'} \int dk\tilde{V}_{\nu\nu'}(k)[2\rho_{Rs\nu}(k)\rho_{Ls'\nu'}(-k) + \rho_{Rs\nu}(k)\rho_{Rs'\nu'}(-k)+\rho_{Ls\nu}(k)\rho_{Ls'\nu'}(-k)], \qquad (6)$$

$$H_{\rm tun}=\lambda\sum_s \int dx\Psi_{su}^{\dagger}\Psi_{sl}e^{-iq_Bx}+{\rm H.c.}, \qquad (7)$$

where s and s' are spin indices, $\Psi_{s\nu}$ is the spin-s electron field operator, $\Psi_{Rs\nu}$ and $\Psi_{Ls\nu}$ are the field operators for the right and left movers, respectively, $\Psi_{s\nu}=e^{ik_{{\rm F}\nu}x}\Psi_{Rs\nu}+e^{-ik_{{\rm F}\nu}x}\Psi_{Ls\nu}$, $\rho_{Rs\nu}(k)=\int dx e^{ikx}\Psi_{Rs\nu}^{\dagger}\Psi_{Rs\nu}$ is the density-fluctuation operator for the spin-s right movers (and analogously for the left movers), and $\tilde{V}_{\nu\nu'}(k)=\int dx e^{ikx}V_{\nu\nu'}(x)$ is the Fourier transform of the two-particle interaction potential $V_{\nu\nu'}(x)$. Writing $H_{\rm int}$ in terms of the interactions between electrons of fixed chirality in Eq. (6) is possible after restricting electron correlations to small momentum-transfer scattering, e.g., if $\tilde{V}(k)\propto\exp(-r_c|k|)$ with $1/r_c \ll k_{\rm F}$. (By making this approximation we disregard backward and umklapp scattering processes, which are thought to be unimportant in our cleaved-wire structure, see, e.g., Ref. 6.)

The 1D-2D scattering randomizes the direction of the 1D electrons in the top quantum well with a mean free path $l_{\rm 1D\text{-}2D}\approx 6\ \mu$m.[13] In infinite wires, this weak scattering can be taken into account by rounding the 1D electron-gas spectral function by a Lorentzian of half width $\Gamma=1/(2\tau_{\rm 1D\text{-}2D})$, where $\tau_{\rm 1D\text{-}2D}$ is the 1D-2D scattering time.

If there were no interactions between the wires, i.e., $V_{ul}\equiv 0$, low-energy spin and charge excitations in each wire would propagate with velocities $v_{s\nu}=v_{{\rm F}\nu}$ and $v_{c\nu}=v_{{\rm F}\nu}/g_{\nu}$, respectively. The parameters g_{ν} can be obtained by bosonization as

$$g_{\nu}=\left[1+\frac{2\tilde{V}_{\nu\nu}(0)}{\pi\hbar v_{{\rm F}\nu}}\right]^{-1/2}<1, \qquad (8)$$

in the case of repulsive interactions, $\tilde{V}_{\nu\nu}(0)>0$. In the limit of a free-electron gas, $\tilde{V}_{\nu\nu}(0)=0$, $g_{\nu}=1$.

We treat tunneling between the wires to lowest order in perturbation theory. Mesoscopic charging effects, such as discussed in, e.g., Ref. 11, are disregarded in our analysis. The current (for electrons of each spin) is given by

$$I=e|\lambda|^2\int_{-\infty}^{\infty}dxdx'\int_{-\infty}^{\infty}dte^{iq_B(x-x')}e^{ieVt/\hbar}C(x,x';t), \qquad (9)$$

where $C(x,x';t)$ is a two-point Green function,

$$C(x,x';t)=\langle[\Psi_l^\dagger\Psi_u(x,t),\Psi_u^\dagger\Psi_l(x',0)]\rangle. \tag{10}$$

In the limit of vanishing interactions between the wires, it reduces to

$$C(x,x';t)=G_u^>(x,t;x',0)G_l^<(x',0;x,t) - G_u^<(x,t;x',0)G_l^>(x',0;x,t) \tag{11}$$

expressed in terms of the one-particle correlation functions

$$G_\nu^>(x,t;x',t')=-i\langle\Psi_\nu(x,t)\Psi_\nu^\dagger(x',t')\rangle, \tag{12}$$

$$G_\nu^<(x,t;x',t')=i\langle\Psi_\nu^\dagger(x',t')\Psi_\nu(x,t)\rangle. \tag{13}$$

Note: Throughout this paper, as in the above equations, the correlation functions are defined for electrons with a fixed spin orientation and the spin index is therefore omitted. The results of this section also hold for direct 2DEG-1D tunneling, if we define $\Psi_{su}(x,t)$ as the field operator for the 2DEG at the edge of the upper quantum well.

B. Interference pattern

As discussed in Sec. III B, the breaking of translational invariance due to the finite size of the tunneling junction can result in an oscillatory dependence of the conductance G on voltage bias V and magnetic field B. In this section we discuss in detail this behavior that arises due to interference of electrons tunneling through a finite-size window. We show that our theoretical framework can quantitatively explain the conductance oscillations observed near the crossing points.

In the following, we mainly focus on the analysis of very distinct interference patterns measured at low magnetic fields (as in Figs. 3 and 4). In Sec. IV B 3 we briefly comment on the conductance near the upper crossing point at high fields (as in Fig. 5). It appears likely that while in the former regime the translational invariance is broken due to the finiteness of the tunneling region only, in the latter case some other mechanisms may also play an important role.

In the actual experiments, several 1D electron modes are occupied in the wires. Here we consider only tunneling between modes which have the lowest energy of transverse motion, and hence the largest Fermi momentum along the wire, namely, $|u_1\rangle$ and $|l_1\rangle$. These modes have densities that differ by only a few percent (see Ref. 5). We thus make a simplifying approximation $v_{\mathrm{Fu}}=v_{\mathrm{Fl}}=v_{\mathrm{F}}$, which is justified by the measured dispersion slopes.[5]

1. Asymmetry due to soft boundaries

In Ref. 8 we showed that the observed asymmetry of the secondary oscillation peaks on the two sides of the main dispersion curves (see Figs. 3 and 4) can be explained within a noninteracting electron picture and assuming a soft confining potential $U_u(x)$ for the upper wire. Here we will employ the model developed there to quantitatively study the form of $U_u(x)$.

Using the phenomenological tunneling Hamiltonian (7), we express the current through the junction at zero temperature as

$$I\propto\mathrm{sgn}(V)\sum_m |M(n,q_B,V)|^2 \tag{14}$$

in terms of the tunneling matrix element

$$M(n,q_B,V)=\int dx\,\psi_n^*(x)e^{-iq_Bx}\varphi_{k_l}(x) \tag{15}$$

between the upper-wire state ψ_n and the lower-wire state φ_{k_l}, the energy of which is lower by eV. The summation in Eq. (14) is over the integers $[\mathrm{sgn}(V)-1]/2<m<e|V|L/(\pi\hbar v_{\mathrm{F}})$ denoting the offset of the ψ_n index $n=n_{\mathrm{F}}+\mathrm{sgn}(V)m$ with respect to the state $\psi_{n_{\mathrm{F}}}$ just below the Fermi energy of the upper wire (and linearizing the dispersions near the Fermi points, assuming $e|V|$ is not too large). The current (14) can be expressed by a single sum because the states of the confined upper wire are discrete, while the states in the lower wire $\varphi_{k_l}(x)=e^{\pm ik_lx}$ can be indexed by a continuous-wave vector k_l. [As in Ref. 8, it is assumed that the left boundary $U_l(x)$ of the lower wire lies outside the tunneling region.] Since the Zeeman energy in GaAs is small, we ignore the spin degrees of freedom.

We argued[8] that for practical purposes of understanding our measurements, the sum in Eq. (14) can be replaced by an integral

$$I\propto\int_0^{eV}d\epsilon|M(E_{\mathrm{Fu}}+\epsilon,q_B,V)|^2, \tag{16}$$

labeling states in the upper wire by energy ϵ with respect to the Fermi energy E_{Fu}. For the conductance obtained by differentiating the current, this approximation will smear out the δ functions appearing when the chemical potential of the upper wire crosses each discrete energy level. Physically, such smearing can be caused by 1D-2D scattering and finite temperature, but even at low temperatures and vanishing scattering the result obtained by integration [Eq. (16)] will not be far off from that found by summation [Eq. (14)] since the dominant contribution to the oscillation pattern near the lower crossing point comes from differentiating the summand in Eq. (14) [or correspondingly the integrand in Eq. (16)], as explained below.

We linearize the dispersions about the Fermi wave vectors $k_{\mathrm{F}\nu}$, so that k_l is given by $(k_l-k_{\mathrm{Fl}})v_{\mathrm{F}}=(\epsilon-eV)/\hbar$. The wave vector inside the upper wire similarly depends on energy: $(k_u-k_{\mathrm{Fu}})v_{\mathrm{F}}=\epsilon/\hbar$. The matrix element squared $|M(E_{\mathrm{Fu}}+\epsilon,q_B,V)|^2$ can then be written as a sum of contributions due to tunneling between right movers and between left movers,

$$|M(E_{\mathrm{Fu}}+\epsilon,q_B,V)|^2=|M(\kappa_+)|^2+|M(\kappa_-)|^2, \tag{17}$$

where $\kappa_\pm=k_u-k_l\pm q_B=\Delta k_{\mathrm{F}}+eV/(\hbar v_{\mathrm{F}})\pm q_B$ and $\Delta k_{\mathrm{F}}=k_{\mathrm{Fu}}-k_{\mathrm{Fl}}$. The tunneling matrix element

$$M(\kappa)=\int dx e^{i\kappa x}\psi_u(x)e^{-ik_{\mathrm{Fu}}x} \tag{18}$$

is determined by the form of the bound-state wave function $\psi_u(x)$ at the Fermi level of the upper wire. We wrote the right-hand side of Eq. (17) as an incoherent sum of the contributions of the two chiralities. This is an approximation we make by disregarding additional interference arising due to the reflection of electrons in the lower wire under gate $\mathcal{G}_1$ (i.e., by the potential U_l in Fig. 7). Taking the latter into account does not considerably affect our results.

$|M(\kappa_\pm)|^2$ do not depend on energy ϵ, and the current (16) can, therefore, be written as[8]

$$I\propto V[|M(\kappa_+)|^2+|M(\kappa_-)|^2]. \tag{19}$$

The differential conductance $G=\partial I/\partial V$ corresponding to the current $I\propto V|M(V)|^2$ becomes $G\propto|M(V)|^2+V\partial|M(V)|^2/\partial V$. If, for example, the oscillatory component of $|M(V)|^2$ has the form $\sin(\mathrm{const}\times V)$, the amplitude of the second term in the conductance will be $2\pi N$ times larger than the amplitude of the first term after N periods of oscillation. The dominant contribution to the oscillatory component of the conductance near the lower crossing point is thus

$$G\propto V\frac{\partial}{\partial V}[|M(\kappa_+)|^2+|M(\kappa_-)|^2]. \tag{20}$$

If the upper-wire confining potential U_u is smooth enough so that the states at the Fermi energy can be evaluated by the WKB approximation, the form of $M(\kappa)$ [Eq. (18)] can be studied both numerically and analytically.[8] In the region between the classical turning points,

$$\psi_u(x)=\frac{1}{\sqrt{k_u(x)}}e^{ik_{\mathrm{Fu}}x}e^{-is(x)}, \tag{21}$$

where $k_u(x)=k_{\mathrm{Fu}}[1-U_u(x)/E_{\mathrm{Fu}}]^{1/2}$ and $s(x)=\int_0^x dx'[k_{\mathrm{Fu}}-k_u(x')]$. In the stationary-phase approximation (SPA), $M(\kappa)$ is evaluated near positions $x^\pm$ $(x^+>x^-)$ where $k_u(x^\pm)=k_{\mathrm{Fu}}-\kappa$ and the integrand in Eq. (18) has a stationary phase. In the case of a symmetric potential, $U_u(x)=U_u(-x)$, the SPA gives

$$M(\kappa)\propto\frac{\Theta(\kappa)}{\sqrt{U_u'(x^+)}}\cos[\kappa x^+-s(x^+)-\pi/4], \tag{22}$$

where $\Theta(\kappa)$ is the Heaviside step function, and the prime in U_u' denotes the derivative. The SPA approximation (22) diverges for small values of κ and we have to resort to a numerical calculation of the integral in Eq. (18).[8] Figure 8 shows the calculated $|M(\kappa)|^2$.

We study the profile of confinement $U_u(x)$ by measuring the period $\Delta\kappa$ of the $|M(\kappa)|^2$ oscillations as a function of κ. In a square well of length L, this period is given by $2\pi/L$. In a soft confinement, the interference stems from the oscillations of the electron wave function near the classical turning points, so that $\Delta\kappa\approx 2\pi/(x^+-x^-)$. For a potential of the form

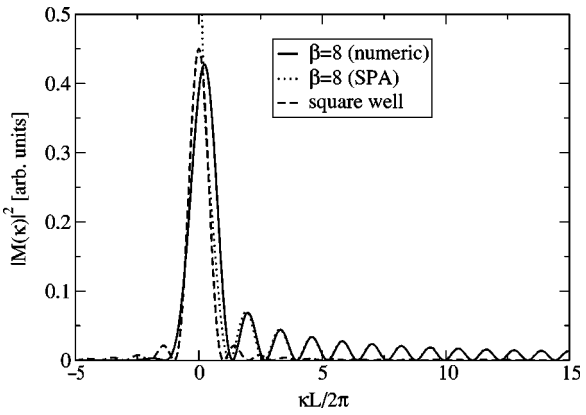

FIG. 8. $|M(\kappa)|^2$ obtained using wave function ψ_u for the 100th WKB state in the potential well [Eq. (23) with $\beta=8$] of the upper wire. The solid line is the numerical calculation, the dotted line is the SPA approximation [Eq. (22)], and the dashed line shows the result for the square-well confinement, for comparison.

$$U_u(x)=E_{\mathrm{Fu}}\left|\frac{2x}{L}\right|^\beta \tag{23}$$

(where β characterizes the ratio between the total length of the upper wire and the extent of its boundaries),[14] $2x^+/L\approx(2\kappa/k_{\mathrm{F}})^{1/\beta}$ for $\kappa>0$ assuming that $\Delta k_{\mathrm{F}}\ll k_{\mathrm{F}}=(k_{\mathrm{Fu}}+k_{\mathrm{Fl}})/2$ (Ref. 8) ($x^-=-x^+$ for a symmetric potential) and the period is therefore given by $\Delta\kappa\approx(2\pi/L)(k_{\mathrm{F}}/2\kappa)^{1/\beta}$. Experimentally, we extract $\Delta\kappa$ by measuring the distance between oscillation zeros in region II of the interference shown in Fig. 3. In order to reduce the statistical uncertainty, the conductance was averaged along lines of constant κ_+, separately for positive and negative bias. In terms of variable $S=\hbar\kappa_+/ed$ (which reduces to magnetic field B at zero voltage and vanishing Δk_{F}),

$$\Delta S\approx\frac{2\pi\hbar}{edL}\left(\frac{\hbar k_{\mathrm{F}}}{2edS}\right)^{1/\beta}. \tag{24}$$

This ΔS is compared with the data in Fig. 9 for several

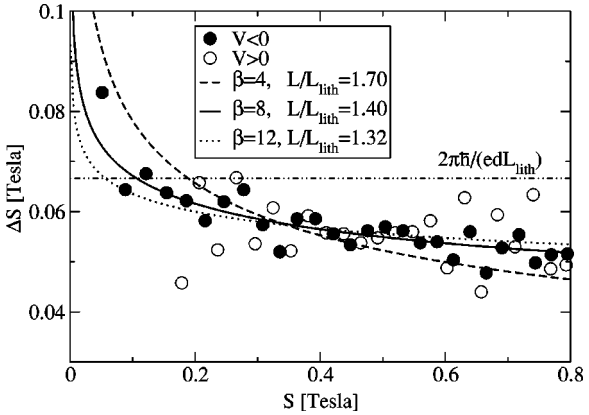

FIG. 9. Period of (faster) oscillations in region II of Fig. 3 as a function of $S=\hbar\kappa_+/(ed)$. Circles show measurements at positive and negative bias and the curves are fits using Eq. (24) at several values of β. The best overall fit is reached at $\beta\approx 7.67$ and $L/L_{\mathrm{lith}}\approx 1.41$, where $L_{\mathrm{lith}}=2\ \mu$m.

values of β (we extract $k_F \approx 1.5\times 10^8$ m^{-1} using measured electron densities[5]). At each β shown in the figure, the distance L was found by the best (least-squares) fit of the curve (24) to the measurements. The lithographic length for the junction was $L_{\rm lith}=2$ μm and the width $d=31$ nm. Such fitting allows us to extract two quantities, $L/L_{\rm lith}=1.45\pm 0.1$ and $\beta=8\pm 2$, characterizing the extent of the 1D confinement and the sharpness of the potential-well boundaries, respectively. It appears that the effective length of the upper wire [defined as the distance between the classical turning points, see Eq. (23)] L is actually about a micron longer than the lithographic length. This conclusion is relatively insensitive to the fitting procedure, since ΔS in Eq. (24) approaches $2\pi\hbar/(edL)$ for $S \gtrsim \hbar k_F/(2ed)$ if the exponent $1/\beta$ is small. The difference between L and $L_{\rm lith}$ can be due to significant screening of the tungsten gates (which are positioned 0.5 μm above the junction) by the 2DEG in the upper quantum well, as viewed by the upper-wire electronic bands.

As a consistency check for the result of the fit in Fig. 9, we performed an analysis of the conductance oscillations that takes into account the dependence on β. According to the $S^{-1/\beta}$ scaling of the oscillations' period, see Eq. (24), and the $S^{1/\beta-1}$ falloff of their amplitude [which follows from Eq. (22), also see Ref. 8], the function $S^{1-1/\beta}G(V,S^{1+1/\beta})$ is periodic in $S^{1+1/\beta}$. Fourier analyzing it at a fixed V, and setting $\beta=8$, we obtained a main peak, the position of which depends very weakly on V, which corresponds to a length of $L=2.81\pm 0.02$ μm, in agreement with the result of the fit. In Fig. 3(b) we plot the absolute value of the main peak, which is seen to decay on a scale of a few mV. We discuss this decay in Sec. IV B 4. For comparison, we also Fourier analyzed the data in Fig. 4(a). For that we found that one has to use a larger value, $\beta=21.5$, in order to obtain a relatively voltage-independent position of the peak. This value of β is reasonable because it gives approximately the same boundary profile for a 6-μm (upper) wire as $\beta=8$ gives for a 2-μm wire.[14] Again we obtained a reasonable length ($L=7.3\pm 0.3$ μm) that varied only weakly as a function of V. The height of the main peak in this case is shown in Fig. 4(b) where it is seen to decay on a faster scale than for the shorter upper wire. The ratio of the scales is approximately the ratio of the upper-wire lengths.

2. Modulation due to spin-charge separation

In the following we describe how electron-electron interactions in the wires and between them affect the oscillation pattern. We show our theoretical results for $G(V,B)$ near the lower crossing point of the $|u_1\rangle \leftrightarrow |l_1\rangle$ transition and compare them to measurements on 2-μm and 6-μm junctions, Figs. 3 and 4. In particular, we find that the difference in the velocities of the charge- and spin-excitation modes in the double-wire system can account for the observed $G(V,B)$ suppression stripes running parallel to the B axis.

As a starting point, let us consider the case in which the interwire interactions are vanishingly small, $V_{ul} \ll V_{ll}$, and the interactions in the two wires are the same, $V_{uu}=V_{ll}$, so that $g_l=g_u=g$, as defined in Eq. (8). For positive voltages $V>0$, the current (9) is then given by

$$I = e|\lambda|^2 \int_{-\infty}^{\infty} dx dx' \int_{-\infty}^{\infty} dt e^{iq_B(x-x')} \times e^{ieVt/\hbar} G_u^{>}(x,t;x',0) G_l^{<}(x',0;x,t). \tag{25}$$

At low magnetic field, the conductance has two main contributions, corresponding to the two edge-state chiralities. The two contributions give bright conductance peaks and sidelobes with opposite slopes, as described in Sec. IV B and Ref. 8. Let us discuss tunneling between the right movers (the current due to tunneling between the left movers at field B equals the tunneling between the right movers at field $-B$). We assume that the electron density in each wire varies slowly on the length scale set by the respective k_F (except for unimportant regions very close to the boundaries). The zero-temperature Green functions entering Eq. (25), in this regime, can be written as[3,4,15]

$$G_{u,l}(x,t;x',0) = \pm \frac{1}{2\pi} \Phi_{u,l}(x,x') \frac{1}{(z - v_F t \pm i0^+)^{1/2}} \times \frac{1}{(z - v_c t \pm i0^+)^{1/2}} \left[\frac{r_c^2}{z^2 - (v_c t \mp i r_c)^2} \right]^{1/2\gamma}, \tag{26}$$

where $v_c = v_F/g$, $\gamma = (g + g^{-1} - 2)/4$, $z = x - x'$, and r_c is a short-distance cutoff (i.e., $1/r_c$ is a momentum-transfer cutoff in the electron-electron interactions). Here, G_u is the $G^>$ Green function (12) for the upper wire and G_l is the $G^<$ Green function (13) for the lower wire. The function Φ_ν is defined by $\Phi_\nu(x,x') = \psi_\nu(x)\psi_\nu^*(x')$, in terms of the WKB wave functions $\psi_\nu(x)$ for right-moving electrons at the Fermi energy in wire ν in a confining potential $U_\nu(x)$ which must be chosen self-consistently to give the correct electron density. Here we assume that $\psi_u(x)$ and $U_u(x)$ are given by Eqs. (21) and (23), while $\psi_l(x) = e^{ik_{Fl}x}$.

Several additional approximations are implied by using Eq. (26) to calculate the tunneling current (25): (i) The weak 1D-2D scattering is neglected, (ii) The voltage is small enough so that one can linearize the noninteracting electron dispersions about the Fermi points and use LL theory (i.e., we disregard the curvature), and (iii) $t \ll v_c L$, so that the discreteness of the energy levels of the upper wire due to electron confinement within a well of length L and their reflection at the boundaries does not considerably modify the LL Green function for an infinite wire [the confinement, however, is manifested in the form of the wave function $\psi_u(x)$; effects due to the discreteness are discussed in Sec. IV B 1 in the regime of noninteracting electrons, and they are believed to be small]. The last approximation breaks down for very low voltages (and, correspondingly, long times) in the regime of the zero-bias anomaly, which is treated separately in Sec. IV C 1.

Substituting Green functions (26) into integral (25), we obtain for the tunneling current

$$I \propto \int_{-\infty}^{\infty} dx dx' e^{i(q_B - k_{\mathrm{Fl}})(x-x')} \psi_u(x) \psi_u^*(x') h(x-x'), \tag{27}$$

using the definition

$$h(z) = -\int_{-\infty}^{\infty} dt \frac{e^{ieVt/\hbar}}{(z - v_{\mathrm{F}} t + i0^+)(z - v_c t + i0^+)} \times \left(\frac{r_c}{z - v_c t + i r_c} \right)^{\gamma} \left(\frac{r_c}{z + v_c t - i r_c} \right)^{\gamma}. \tag{28}$$

The integrand in Eq. (28) has a simple analytic form: It has two first-order poles at $t = z/(v_{\mathrm{F}} + i0^+)$ and $t = z/(v_c + i0^+)$ and two branch cuts starting with singularities at $t = (\pm z + i r_c)/v_c$. The contour of integration can be deformed leaving two nonvanishing contributions: $h(z) = h_1(z) + h_2(z)$. The first contribution, $h_1(z)$, is due to integration around the poles,

$$h_1(z) = \frac{2\pi i e^{ieVz/(\hbar v_c)}}{(v_c - v_{\mathrm{F}})(z + i0^+)} \left(\frac{r_c^2}{r_c^2 + 2izr_c} \right)^{\gamma} - \frac{2\pi i e^{ieVz/(\hbar v_{\mathrm{F}})}}{(v_c - v_{\mathrm{F}})(z + i0^+)} \times \left\{ \frac{r_c^2}{r_c^2 + z^2[1 - (v_c/v_{\mathrm{F}})^2] + 2izr_c v_c / v_{\mathrm{F}}} \right\}^{\gamma}, \tag{29}$$

and the second contribution, $h_2(z)$, is due to integration around the branch cuts. For $z > 0$, for example,

$$h_2(z) = 2i \sin(\gamma\pi) e^{-eVr_c/(\hbar v_c)} \times \left\{ \int_{z/v_c}^{\infty} - \int_{-\infty}^{-z/v_c} \right\} dt \left[\frac{r_c^2}{(v_c t)^2 - z^2} \right]^{\gamma} \times \frac{e^{ieVt/\hbar}}{(z - v_c t - i r_c)(z - v_{\mathrm{F}} t - i r_c v_{\mathrm{F}}/v_c)}. \tag{30}$$

In our system we expect that[5] $g \approx 0.7$, so that $\gamma \approx 0.03 \ll 1$. Therefore, since $r_c \sim 30$ nm (the width of the wires) and $z < L \approx 2-6$ μm, the terms of the form $(\cdots)^{\gamma}$ in Eq. (29) can be safely ignored (except for the regime of extremely low voltages, which is discussed in Sec. IV C 1). Furthermore, $h_2(z) \ll h_1(z)$, so that we arrive at an approximation

$$h(z) \approx -2\pi i \frac{e^{ieVz/(\hbar v_{\mathrm{F}})} - e^{ieVz/(\hbar v_c)}}{(v_c - v_{\mathrm{F}})(z + i0^+)}. \tag{31}$$

Substituting this into Eq. (27), we can now evaluate the current. One notices that after making the approximation (31), the current (27) becomes the same as if there were no electron-electron interactions but different Fermi velocities in the two wires, given by v_{F} and v_c. Using Eqs. (27) and (31), we, finally, get for the conductance $G = \partial I / \partial V$:

$$G(V,B) \propto \frac{1}{v_c - v_{\mathrm{F}}} \left[\frac{1}{v_{\mathrm{F}}} |M(\kappa_{\mathrm{F}})|^2 - \frac{1}{v_c} |M(\kappa_c)|^2 \right], \tag{32}$$

where $\kappa_{\mathrm{F,c}} = q_B + \Delta k_{\mathrm{F}} + eV/(\hbar v_{\mathrm{F,c}})$ and $M(\kappa)$ is given by Eq. (18).

If the excitation velocities in the wires are nearly the same, $v_{\mathrm{F}} \approx v_c = v$, we can approximate the conductance (32) by

$$G \propto \frac{\partial}{\partial \eta} \eta |M(\eta, V)|^2 = |M(\kappa)|^2 + V \frac{\partial}{\partial V} |M(\kappa)|^2, \tag{33}$$

where $M(\eta, V) = M(q_B + \Delta k_{\mathrm{F}} + \eta V)$ and $\eta = e/(\hbar v)$. This reproduces Eq. (19). One can refine the form of the second term on the right-hand side of Eq. (33) (which can be much larger than the first term, see Sec. IV B 1), using approximation (22), when the difference between velocities v_{F} and v_c becomes appreciable (which is the case for $g \approx 0.7$):

$$\tilde{G} \propto \frac{\Theta(\kappa)}{U_u'(x^+)} \cdot \frac{\sin[eVx^+(1/v_{\mathrm{F}} - 1/v_c)/\hbar]}{1/v_{\mathrm{F}} - 1/v_c} \times \cos 2[\kappa x^+ - s(x^+)]. \tag{34}$$

Here, κ and x^+ are defined using velocity $v = 2(1/v_{\mathrm{F}} + 1/v_c)^{-1}$, and $\tilde{G}$ stands for the second contribution to the conductance in Eq. (33). At low bias, $\tilde{G} \to 0$ linearly in V and the term $G \propto |M(\kappa)|^2$ governs the conductance. This contribution is further suppressed as V^{α} (at zero temperature) in the zero-bias anomaly regime discussed in Sec. IV C 1.

We can generalize the preceding discussion of this section to include interactions between the wires, i.e., $V_{ul} \neq 0$. Since the quantum wires are closely spaced, the interwire interactions can be sizable. Furthermore, because the Fermi velocities in modes $|u_1\rangle$ and $|l_1\rangle$ are similar, the excitations in the coupled wires can propagate with velocities quite different from those in the isolated wires. When we take V_{ul} into account, the dominant part of the Green function (10) becomes (assuming weak interactions, in the spirit of the preceding discussion) (Ref. 7)

$$C(x,x';t+i0^+) \propto -\frac{\Phi_u \Phi_l^*(x,x')}{(z - v_{\mathrm{Fu}} t)^{1/2} (z - v_{\mathrm{Fl}} t)^{1/2}} \times \frac{1}{(z - v_{c-} t)^{(1/2)+\theta_r} (z - v_{c+} t)^{(1/2)-\theta_r}}, \tag{35}$$

where

$$v_{c\pm} \approx \frac{v_{cu} + v_{cl}}{2} \pm \frac{\tilde{V}_{ul}(0)}{\pi\hbar} \sqrt{1 + r^2}. \tag{36}$$

Here, $r = \pi(v_{cu} - v_{cl})/2\tilde{V}_{ul}(0)$ and $\theta_r = 1/(2\sqrt{1+r^2})$ is finite for nonvanishing interactions between the wires, and v_{cn} are the charge-excitation velocities in the isolated wires. [Note that there appears to be a sign error in Ref. 7 in the

expression for the velocities $v_{c\pm}$ in the physical case of repulsive interactions $\tilde{V}_{ul}(0)>0$.]

For a symmetric double-wire system, $v_{\mathrm{Fu}}=v_{\mathrm{Fl}}=v_{\mathrm{F}}$, $V_{uu}\equiv V_{ll}$, and $v_{cu}=v_{cl}$, so that $r=0$ and $\theta_r=1/2$. (In this case, v_{c+} and v_{c-} become the velocities of the symmetric and antisymmetric charge excitations, respectively.) The Green function then reduces to $C\propto-\Phi_u\Phi_l^*(z-v_{\mathrm{F}}t)^{-1}(z-v_{c-}t)^{-1}$ and we reproduce our main result of this section, Eq. (32), after replacing v_c with the antisymmetric charge-excitation velocity v_{c-}. This is natural since tunneling in a symmetric biwire can only excite the antisymmetric modes at low magnetic fields.

In addition to the structure studied in Sec. IV B 1 for the system of noninteracting electrons, we now show that the electron-electron interactions in the wires lead to a modulation of the conductance oscillations along the voltage axis.[8] This modulation suppresses the contribution $\tilde{G}$ [Eq. (34)] to zero in stripes parallel to the field axis. The distance between them is

$$\Delta V_{\mathrm{mod}}=\frac{\pi\hbar v_{c-}v_{\mathrm{F}}}{ex^{+}(v_{c-}-v_{\mathrm{F}})}. \tag{37}$$

The ratio between ΔV_{mod} and the period

$$\Delta V=\frac{2\pi\hbar v_{c-}v_{\mathrm{F}}}{ex^{+}(v_{c-}+v_{\mathrm{F}})} \tag{38}$$

due to the wave-function oscillations near the turning points [compare to Eq. (3)]

$$\frac{\Delta V_{\mathrm{mod}}}{\Delta V}=\frac{1}{2}\frac{v_{c-}+v_{\mathrm{F}}}{v_{c-}-v_{\mathrm{F}}}=\frac{1}{2}\frac{1+g_-}{1-g_-} \tag{39}$$

can be used as an independent measure of the interaction parameter $g_-=v_{\mathrm{F}}/v_{c-}$. From Figs. 3(a) and 4(a), we find that

$$g_-=0.67\pm0.07, \tag{40}$$

similarly to the value for g_l obtained by the zero-bias anomaly in Sec. IV C 2. Also, from Eq. (34) it follows that the oscillation pattern [of the principal term $\tilde{G}(V,B)$] gains a π-phase shift across each suppression strip. Such phase shifts can also be seen in experimental Figs. 3(a) and 4(a).

Finally, we compare the interference pattern predicted by our theory, Eq. (32), with the experiment, Figs. 3(a) and 4(a). $G(V,B)$ calculated using a smooth confining potential [Eq. (23) with $\beta=8$] for the upper wire is shown in Fig. 10. Many pronounced features observed experimentally—the asymmetry of the sidelobes, a slow falloff of the oscillation amplitude and period away from the principal peaks, an interference modulation along the V axis, and π-phase shifts at the oscillation suppression stripes running parallel to the field axis—are reproduced by the theory.

In Fig. 11, we repeat the calculation using $\beta=22$, which defines potential (23) with a similar boundary profile near the turning points of a three-times longer wire.[14] (Here by length we mean the distance between the classical turning points,

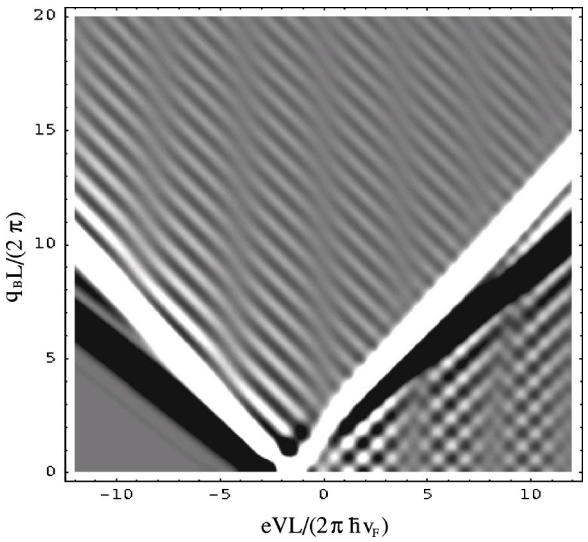

FIG. 10. The differential conductance interference pattern near the lower crossing point calculated by Eq. (32) for tunneling between right movers (and similarly for left movers) using a smooth confining potential for the upper wire, Eq. (23). $v_{c-}=1.4v_{\mathrm{F}}$, $\Delta k_{\mathrm{F}}=4\pi/L$, and $\beta=8$. We used the numerically found $|M(\kappa)|^2$, also shown in Fig. 8. The figure must be compared to experimental Fig. 3.

which, as explained in Sec. IV B 1, can be somewhat different from the lithographic length.) Again an agreement between the predicted (Fig. 11) and measured (Fig. 4) oscillation patterns is apparent. In Fig. 11 a few weak sidelobes also appear to the left of the main dispersion peaks, unlike in Fig. 10 where they appear strictly to the right. In addition, the interference modulation in the voltage direction has sharper features in Fig. 11. These trends are expected for longer junctions as the boundaries become steeper on the scale set by the total length.

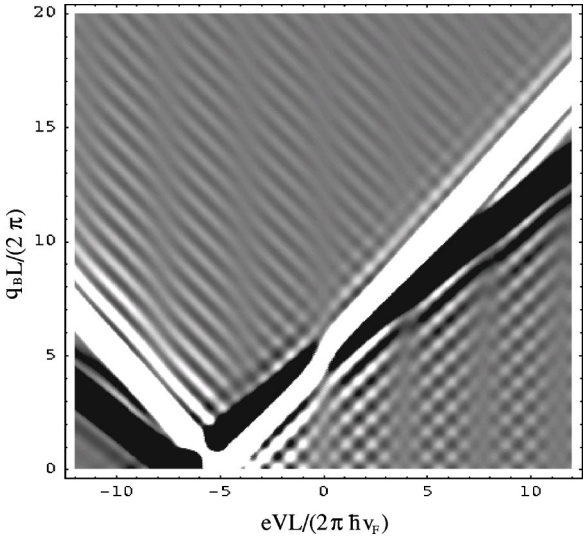

FIG. 11. Same as Fig. 10 but with $\Delta k_{\mathrm{F}}=10\pi/L$ and $\beta=22$, describing a longer junction with a similar boundary profile. $|M(\kappa)|^2$ was correspondingly recomputed (now putting 300 electrons per spin in the upper wire). The figure must be compared to experimental Fig. 4.

Tunneling between 1D channels with different Fermi velocities can also yield an interference modulation similar to that described in this section even when the electron-electron interactions are vanishingly small.[17] It is thus important to emphasize that we suggest the spin-charge separation picture to explain this modulation relying on the experimental result (see Ref. 5) that the densities of modes $|u_1\rangle$, $|l_1\rangle$ and, therefore, the corresponding Fermi velocities are nearly identical.

Using Eq. (35) we also studied various possible scenarios in which the interactions in the two wires differ. For example, in a situation in which the upper wire is perfectly screened, so that $V_{uu}, V_{ul} \equiv 0$, there are still two velocities present in the system, v_F and v_{cl}, but the interference pattern is qualitatively very different from that shown in Fig. 10 and observed experimentally [see Figs. 3 and 4]. Since a considerable weight of the charge-excitation contribution to the tunneling strength is shifted to velocity v_F (which is now also the charge-excitation velocity in the upper wire), the oscillation pattern does not exhibit the pronounced vertical suppression stripes, but rather a much weaker modulation. The same conclusion also holds for intermediate regimes of relative screening in the two wires, when the system is not symmetric and the two charge-excitation velocities significantly differ. The pronounced suppression stripes are, therefore, present only if most of the charge-excitation tunneling weight is peaked at a single velocity v_{c-} (which is guaranteed only when the system is nearly symmetric).

Taking into account 1D-2D scattering in the upper quantum wire will smear out the oscillation pattern by its convolution with a Lorentzian in the B direction, similarly to Eq. (52) below. The corresponding effect is, however, small because of the high quality of our wires, which have a long scattering length,[13] $l_{1D\text{-}2D} \approx 6\ \mu$m.

3. Upper crossing point

In practice, since the fields necessary to reach the upper crossing point are quite large (e.g., 7 T for the $|u_1\rangle \leftrightarrow |l_1\rangle$ transition), even atomic-scale disorder in the junction can lead to a significant variation δq_B of the momentum transfer along the tunneling region. In particular, $\delta q_B = eB\,\delta d$ can be comparable with $2\pi/L$, the reciprocal wave vector of the upper wire. This can significantly broaden the principal dispersion peaks. Furthermore, Zeeman splitting becomes about a percent of the Fermi energy at these high fields and results in somewhat different dispersions for different spin modes. Away from the main peaks, however, we still expect to see sidelobes due to stationary phases at the ends of the junction, similarly to the regime of low magnetic fields discussed above (with possibly a faster decoherence in the V direction than just due to the dispersion curvature studied in Sec. IV B 4). Such oscillations [with about the period (3)] are indeed observed experimentally, as can be seen in Fig. 5. Because of the mentioned complications, we, nevertheless, do not pursue a detailed analysis of the conductance near the upper crossing point in this paper.

4. Dephasing of the oscillations

It is evident from Figs. 3(a) and 4(a) that the interference decays as $|V|$ is increased. A more quantitative analysis of this decay is shown in Figs. 3(b) and 4(b), where the amplitude of the oscillations is plotted as a function of voltage. It is clear that the measured modulation has a fast-decaying envelope, which cannot be explained by the analysis of Sec. IV B 2. [See, for example, Eq. (34) which predicts that the modulation is roughly periodic.]

One scenario for the dephasing occurs even in the case of *noninteracting* electrons considered in Sec. IV B 1, at which time we take the finite curvature of the single-particle dispersions into account. Let us return to the form of the current in Eq. (16):

$$I \propto \int_0^{eV} d\epsilon [|M(\kappa_+)|^2 + |M(\kappa_-)|^2]. \tag{41}$$

Correcting our previous results to take into account the nonlinear dispersion near the Fermi points, we now write $\kappa_\pm = [k_{Fu}^2 + 2m\epsilon/\hbar^2]^{1/2} - [k_{Fl}^2 + 2m(\epsilon - eV)/\hbar^2]^{1/2} \pm q_B$. [Using Eq. (41) we still imply low enough bias V, so that the densities of states in the wires are relatively constant on the energy scale of $e|V|$.] Expanding this expression to lowest order in curvature, we further obtain

$$\kappa_\pm = \Delta k_F + \frac{eV}{\hbar v_F} \pm q_B + \frac{eV(eV - 2\epsilon)}{2\hbar^2 v_F^2 k_F}. \tag{42}$$

[Eq. (19) can be recovered by neglecting the last term above.] The current (41) then becomes

$$I \propto \int_{-eV/2}^{eV/2} d\epsilon \left| M\left(\Delta k_F + \frac{eV}{\hbar v_F} + q_B - \frac{\epsilon eV}{\hbar^2 v_F^2 k_F} \right) \right|^2 + (q_B \to -q_B). \tag{43}$$

It is easy to see now that the contribution to the conductance obtained by differentiating the integrand in Eq. (43) will be suppressed when the argument κ of the tunneling matrix amplitude $M(\kappa)$ changes by the full period of oscillations $\Delta\kappa$ upon energy ϵ variation between the integration limits $\pm eV_{sup}/2$. We thus arrive at the condition for the suppression voltage V_{sup}:

$$\Delta\kappa = \frac{(eV_{sup})^2}{\hbar^2 v_F^2 k_F}. \tag{44}$$

Approximating $\Delta\kappa \approx 2\pi/L$ and translating it into the oscillation period in the bias direction $e\Delta V = \hbar v_F \Delta\kappa$, one finally obtains

$$\frac{V_{sup}}{\Delta V} = \sqrt{\frac{Lk_F}{2\pi}}. \tag{45}$$

Using density 100 μm^{-1} for the lowest bands in the wires,[5] we find $V_{sup}/\Delta V \approx 7$ (≈ 12) for the 2-μm (6-μm) junction. An implicit assumption in the derivation is that we are still close enough to the Fermi level so that higher-order corrections should not modify the result significantly [in particular, for the calculation of the matrix element (18) it is still reasonable to use the wave function $\psi_u(x)$ at the Fermi energy].

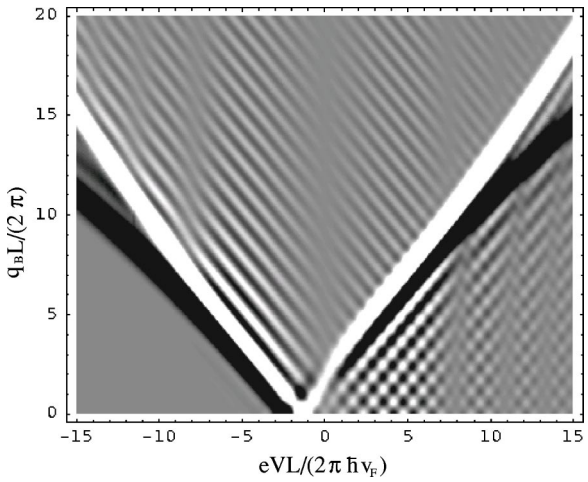

FIG. 12. The differential conductance interference pattern near the lower crossing point calculated by Eq. (43), within the noninteracting electron picture, using the matrix element $M(\kappa)$ shown in Fig. 8 (for $\beta=8$). See text for further details.

The result of the numerical calculation using Eq. (43) and the matrix element $M(\kappa)$ plotted in Fig. 8 (using parameters characteristic for the 2-μm sample) is shown in Fig. 12. Notice that when the voltage exceeds $V_{\rm sup}\approx 7\Delta V$, so that the pattern starts dephasing due to the finite curvature, a beating pattern appears. It differs from the data in several important aspects: First of all, the lines of suppressed $G(V,B)$ are not equidistant. In addition, $V_{\rm sup}$, corresponding to the first suppression stripe (on either the positive- or negative-voltage sides), is about twice larger than the period we observe in Fig. 3(b) and four times larger than that in Fig. 4(b), which in both cases is given by about $3\Delta V$. This suggests that the source of the beating in the experimental data is not the curvature of the dispersions, but rather the spin-charge separation mechanism discussed in Sec. IV B 2.

Another important difference between Eq. (41) and the experiment is that the decay of the oscillations is much stronger in the latter. It might therefore be necessary to consider both the curvature and electron interactions in order to understand the fast decay of the conductance oscillation amplitude with increasing voltage. Taking into account the curvature while bosonizing excitations of the *interacting* electrons[1,2] leads to higher-order terms in the Hamiltonian. Physically this corresponds to interactions between bosonic excitations which therefore acquire a finite lifetime. The singularities of the spectral densities will correspondingly be rounded, in turn smearing the conductance interference pattern. Further complications may arise from the electron backscattering which was entirely disregarded: While the low-energy properties of the system are not affected by the backscattering (apart from rescaling of certain parameters) since it renormalizes downward in the case of repulsive interactions, the story at a finite energy could be different. The reason for this is a slow (logarithmic) renormalization flow of the backscattering strength. If a significant backscattering is present in the original Hamiltonian, it could therefore still be considerable at a finite energy. A detailed study of these effects, however, lies beyond this paper's scope.

C. Zero-bias anomaly

1. Crossing points

It is enlightening to further study tunneling between 1D channels at low bias when the magnetic field is tuned to match two Fermi points of the wires (see Sec. III A). The zero-bias properties are similar near the two crossing points and, for definiteness, we choose to discuss the upper crossing, in which the magnetic wave vector q_B is close to $k_{\rm Fu}+k_{\rm Fl}$ and the field changes the chirality of the tunneling electrons: The tunneling is among the left movers of the upper wire and the right movers of the lower wire. For the $|u_1\rangle\leftrightarrow|l_1\rangle$ transition, this point is located at $B\approx 7$ T, see Fig. 2. The results are straightforward to apply to the regime of the lower crossing point, as well.

For clarity, we start by making a series of simplifying assumptions which will be dropped in subsequent generalizations: First, we set the upper-wire and interwire interactions, V_{uu} and V_{ul}, to zero. Physically, this corresponds to a regime in which the Coulomb interactions in the upper wire are perfectly screened by the 2DEG. Secondly, we further simplify the model by assuming a square-well confinement for the electronic states in the upper quantum wire and an infinitely steep reflecting left boundary for the electrons in the lower wire, i.e., $U_u(x)$ $[U_l(x)]$ is constant for $|x|<L/2$ $[x>-L/2]$ and infinite otherwise. As we showed in the previous sections, both of the above assumptions are not very realistic for the purpose of studying the interference pattern. In the zero-bias anomaly regime, however, they can be a good starting point, at least, for pedagogical reasons.

Electron states participating in tunneling near the crossing points [Eq. (1)] lie close to the Fermi levels in both wires. It is therefore possible to calculate the correlation functions analytically using LL theory, after the dispersion relations in the wires are linearized. At the upper crossing point, we only need to retain Green functions of the left movers of the upper wire and the right movers of the lower wire. At zero temperature these are given by

$$G_u^{>}(x,t+i0^+;x',0)=-\frac{1}{4L}\frac{e^{-ik_{\rm Fu}z}e^{-\Gamma|z|/v_{\rm F}}}{\frac{\pi}{2L}\sin(z+v_{\rm F}t)}$$

$$\overset{L\to\infty}{=}-\frac{1}{2\pi}\frac{e^{-ik_{\rm Fu}z}e^{-\Gamma|z|/v_{\rm F}}}{z+v_{\rm F}t} \qquad (46)$$

for $|x|$, $|x'|<L/2$, and $G_u^{>}$ vanishing otherwise, and

$$G_l^{<}(x',0;x,t+i0^+)=-\frac{1}{2\pi}\frac{e^{-ik_{\rm Fl}z}}{(z-v_{\rm F}t)^{1/2}}\frac{1}{(z-v_{cl}t)^{1/2}}\times\left[\frac{r_c^2}{z^2-(v_{cl}t-ir_c)^2}\right]^{(g_l+g_l^{-1}-2)/8}\times\left[\frac{z'^2-z^2}{z'^2-(v_{cl}t)^2}\right]^{(g_l-g_l^{-1})/8}, \qquad (47)$$

for $x,x' > -L/2$, and vanishing otherwise, where $z = x - x'$, $z' = x + x' + L$, and r_c is a small-distance cutoff. As specified above, Eq. (46) [Eq. (47)] contains only the component for the left (right) movers in the upper (lower) wire; we have thus omitted terms proportional to $e^{ik_F z}$, $e^{ik_F z'}$, and $e^{-ik_F z'}$ which do not contribute constructively to tunneling near the upper crossing point. The last factor in the expression for $G_l^<$ is due to the closed boundary at $x = -L/2$.[16,18,19]

For sufficiently large voltages, $eV \gg 2\hbar v_F/(g_l L)$, the tunneling electrons do not feel the junction boundaries on the time scale set by the voltage. In particular, the left boundary of the lower wire does not affect the dynamics and, effectively, electrons directly tunnel into the bulk of the lower wire: The last term in Eq. (47) is close to unity and can, therefore, be omitted. Terms of the form $1/(z \pm vt)^\vartheta$ entering Eqs. (46) and (47) are dominated by the long-t behavior in the integral [Eq. (25); the voltage is assumed to be positive] if $eV \ll \hbar \max(vq,\Gamma)$, where $q = q_B - (k_{Fu} + k_{Fl})$. The conductance is then suppressed as a power law

$$G(V) \propto V^\alpha \tag{48}$$

with the exponent $\alpha_{bulk} = (g_l + g_l^{-1} - 2)/4$. This result is easy to generalize for the case of unscreened interactions in the upper wire:

$$\alpha_{bulk} = \sum_{\nu = u,l} \frac{g_\nu + g_\nu^{-1} - 2}{4}. \tag{49}$$

If the interwire interactions V_{ul} are also significant, the elementary excitation modes in the wires become coupled and α_{bulk} has a more complicated form than that in Eq. (49).[6] Interference oscillations discussed in Sec. IV B can modulate the power-law current suppression (48), setting an upper voltage bound, $eV < e\Delta V \approx 2\pi\hbar v_F/L$, for the validity of Eq. (48). It would therefore be hard to observe the exact power-law voltage dependence (48) with the exponent (49) in the regime when $eV \gg 2\hbar v_F/(g_l L)$ (see, however, Sec. IV C 2).

If $eV \ll 2\hbar v_F/(g_l L)$, electrons effectively tunnel into the end of the lower wire and the current suppression is governed by processes in the lower wire outside the tunneling region. In particular, details of the interactions in the finite upper wire do not play a role. The last term in Eq. (47) now also contributes to the exponent of the long-t asymptotic, and α in Eq. (48) is given by

$$\alpha_{end} = \frac{g_l^{-1} - 1}{2}. \tag{50}$$

The upper wire, in this case, can be viewed as a point contact and the tunneling exponent is determined entirely by the properties of the lower wire outside the tunneling region.

At a finite temperature, the time scale relevant for the discussion above is set by $\max(eV, k_B T)$. The power law (48) should now be replaced with

$$G(V,T) \propto T^\alpha F_\alpha\left(\frac{eV}{k_B T}\right), \tag{51}$$

where $F_\alpha(x)$ is a known scaling function with properties $F_\alpha(0) = \text{const}$ and $F_\alpha(x) \propto x^\alpha$ in the limit of $x \gg 1$.[12] At low temperatures the conductance yields a low-bias dip extending to voltages $eV \sim k_B T$ with $G(V=0) \propto T^\alpha$.

In Sec. IV B we showed that the conductance $G(V,B)$ exhibits a characteristic interference pattern due to wave-function oscillations near the gates confining the tunneling region. We can easily read out the profile of this pattern for the current (25) using the correlation functions (46) and (47) in the low-energy regime considered in this section (namely, $t \gg z$):

$$G(B) \propto \int_{-\infty}^{\infty} dk \frac{\Gamma/v_F}{k^2 + (\Gamma/v_F)^2} |M(k-q)|^2, \tag{52}$$

where $M(\kappa)$ is the tunneling matrix element, Eq. (18).

The discussion in this section also holds for the lower crossing point, at which the electrons do not change their chirality upon tunneling. To directly apply the above results to this regime (for definiteness, assuming we now consider the transition between the right-moving electrons), we only need to redefine the distance from the crossing point in the field direction: $q = q_B + k_{Fu} - k_{Fl}$ (and analogously for the transition between the left movers).

2. Direct tunneling from the 2DEG

It is straightforward to generalize the main results of the preceding section to the regime of direct tunneling from the 2DEG. Equation (25) stays valid in this case, but now $G_u^>$ is the Green function for the 2DEG near the edge of the upper quantum well. We calculate this correlation function and discuss its limiting behavior at low energies in Appendix B. The 2DEG density of states is finite at the Fermi energy and, therefore, the long-t behavior of the one-particle Green function is $G^>(t) \propto 1/t$. If $\max(eV, k_B T) \ll \hbar v_F k_{F,2D}$, where $\hbar k_{F,2D}$ is the 2DEG Fermi momentum and v_F is the lower of the Fermi velocities of the 1D band and the 2DEG, the temperature and voltage dependence of the differential conductance are governed by the exponents (49), with $g_u = 1$, or Eq. (50), depending on the relation between $\max(eV, k_B T)$ and $2\hbar v_F/(g_l L)$. Because in this regime we tunnel directly from the 2DEG, interactions in the 1D modes of the upper quantum well do not play a role, and both α_{bulk} and α_{end} are determined only by the interaction constant g_l of the lower wire. While the field dependence of the conductance for the direct 2DEG—lower-wire tunneling is different from Eq. (52) (in particular, the conductance does not exhibit a strong oscillation pattern)—the low-energy properties stay similar to the case of the 1D-1D tunneling. In spite of a complicated dependence of $G(V,B)$ on magnetic field, the zero-bias anomaly is pronounced in the data for tunneling either between different 1D bands or between the 2DEG and the 1D bands.

As described in Sec. III C, we measured the zero-voltage conductance dip at temperatures $0.2 < T < 2$ K on a junction of length $L = 6$ μm at $B = 2.5$ T. It can be seen in Fig. 2 that at this magnetic field, the conductance is dominated by direct tunneling from the 2DEG, $|u_3\rangle \leftrightarrow |l_2\rangle$. Since $\hbar v_F k_{F,2D}/k_B$

$\sim 100\ \mathrm{K} \gg T$, the temperature dependence of the zero-bias dip can be used to extract the value of the interaction constant g_l for the band $|l_2\rangle$. The data points and the (best) theoretical fitting curves are shown in Fig. 6; we find

$$g_l = 0.59 \pm 0.03. \tag{53}$$

The transition point between the two lines in the plot is consistent with an estimate $2\hbar v_F/(g_l L k_B) \approx 0.5$ K for the second 1D mode of the lower wire, $|l_2\rangle$.

As a consistency check, we plot in the insets to Fig. 6 curves calculated using Eq. (51) (taking both α_{end} and α_{bulk} for the exponent). g_l and the overall proportionality constants were independently obtained from the power-law temperature dependence of the bottom of the dip, i.e., $G(V=0,T)$, so that at this point we do not have any remaining fitting parameters. The results show reasonable agreement with the data: When $\max(eV,k_BT) > 2\hbar v_F/(g_l L)$ the data is consistent with $\alpha = \alpha_{\mathrm{bulk}}$ while when $\max(eV,k_BT) < 2\hbar v_F/(g_l L)$ it is more consistent with $\alpha = \alpha_{\mathrm{end}}$. Thus, in particular, there is a crossover between α_{end} and α_{bulk} in the data for $G(V)$ at $T = 0.24$ K. For voltages $V \sim 1$ meV that are comparable to the Fermi energies of the modes participating in tunneling, the power-law behavior (51) is replaced by a more complex structure modulated by the dispersions in the wires and the upper well, see Fig. 2.

V. CONCLUSIONS

We have presented a detailed experimental and theoretical investigation of tunneling between two interacting quantum wires of exceptional quality fabricated at the cleaved edge of a GaAs/AlGaAs heterostructure. The study focused on revealing electron-electron interaction effects on the conductance interference pattern arising from the finite size of the tunneling region and the conductance suppression at low voltage.

In the analysis of the data the finiteness of the junction plays a central role. Breaking translational invariance, the boundaries give rise to secondary dispersion peaks in the dependence of the conductance on voltage bias and magnetic field. Smooth gate potentials result in a strongly asymmetric interference profile, while the Coulomb repulsion in the wires leads to spin-charge separation which, in turn, modulates the conductance oscillation amplitude as a function of voltage bias.

Interplay between the electron correlations in the wires and the finiteness of the junction length also results in different regimes of the zero-bias anomaly. At the lowest voltages, the upper wire is effectively a point-contact source for injecting electrons into the semi-infinite lower wire. On the other hand, at higher voltages, electrons effectively tunnel between the bulks of the two wires along the length of the junction.

Using the temperature dependence of the zero-bias dip, we found the value of the interaction parameter $g_l = v_{\mathrm{Fl}}/v_{cl}$ for band $|l_2\rangle$ in the lower wire to be 0.59 ± 0.03. From the ratio between the slow (due to spin-charge separation) and fast (due to upper-wire confinement) scales of the conductance oscillations, we also extracted the interaction parameter $g_- = v_F/v_{c-}$ corresponding to the antisymmetric charge-excitation mode in the lowest bands $|u_1\rangle$ and $|l_1\rangle$ of the biwire to be 0.67 ± 0.07.

While g_- and g_l have similar numerical values, these quantities should be contrasted: g_l is the interaction parameter (8) of the channel $|l_2\rangle$ in the lower wire, which is screened by other 1D states in the wires as well as the 2DEG of the upper quantum well. g_-, on the other hand, is a parameter characterizing the (antisymmetric) charge mode in the coupled $|u_1\rangle$ and $|l_1\rangle$ channels of the two wires, which is relatively weakly screened by the 2DEG since the latter has a smaller Fermi velocity (being, nevertheless, still larger than the Fermi velocity of $|l_2\rangle$).[5] This can explain why g_- and g_l are comparable while $|l_2\rangle$ has about half the Fermi velocity of $|u_1\rangle$ and $|l_1\rangle$. [The interwire interaction would only enhance the mismatch as it reduces v_{c-}, see Eq. (36).]

Similar values for the interaction parameter g, in the range between 0.66 and 0.82, were found in Ref. 20 for single cleaved-edge quantum wires by measuring the temperature dependence of the linewidth of resonant tunneling through a localized impurity state. Spectral properties of the same double-wire structure as reported here were investigated in Ref. 5, also indicating comparable values of g, about 0.75, for various intermode transitions. An interaction parameter $g \approx 0.4$ was found for GaAs quantum-wire stacks in resonant Raman-scattering experiments;[21] the smaller value of g there can be attributed to much lower electron densities and no screening by the 2DEG, as in our measurements.

ACKNOWLEDGEMENT

We have enjoyed illuminating discussions with Y. Oreg and A. Stern. This work was supported in part by the US-Israel BSF, NSF Grant No. DMR 02-33773, and by a research grant from the Fusfeld Research Fund. O.M.A. is supported by a grant from the Israeli Ministry of Science.

APPENDIX A: INDEPENDENT-MODE APPROXIMATION

In our analysis we treat different 1D bands in the wires as independent and disregard interband interactions. While this is a convenient approximation for theoretical investigations that has been often assumed in previous works,[5–8] it needs to be further justified. Tunneling into multimode 1D wires was considered in Ref. 22. It was shown that low-energy tunneling into the edge of a semi-infinite wire with N bands is governed by the tunneling density of states exponents α_i such that the differential conductance (at zero temperature and low voltage V) is given by $G \propto \Sigma_{i=1}^{N} |t_i|^2 V^{\alpha_i}$, where t_i is the tunneling amplitude for the ith mode. In the independent-mode approximation with interactions described by Hamiltonian (6) for each mode, these exponents are given by Eq. (50) with the parameter g describing interactions in each mode. On the other hand, in a more realistic picture one deals with an interaction Hamiltonian

$$H_{\mathrm{int}} = \frac{V_0}{2} \sum_{i,j=1}^{N} \int_0^\infty dx \rho_i(x) \rho_j(x), \tag{A1}$$

which takes into account the interband coupling. Here, V_0 is the zero-momentum Fourier component of the interaction potential $V(x)=V_0\delta(x)$ and ρ_i is the electron density in the ith band. The exact form of the potential is not important since we are only interested in the long-wavelength quantum fluctuations.[22]

The exponents are given by[22] $\alpha_i=(\Sigma_{l=1}^{N}\gamma_{il}^2 s_l/v_i)-1$, where v_i is the Fermi velocity of the noninteracting 1D electron gas at the density of the ith mode, s_l is the velocity of the lth soundlike excitation in the presence of the potential $V(x)$, and γ_{il} characterizes coupling between the ith and lth noninteracting modes after the interaction potential $V(x)$ is switched on. In the case of a single transverse mode with spin degeneracy, $N=2$, $\gamma_{il}^2=1/2$, and $s_1=v_F\sqrt{1+2V_0/(\pi\hbar v_F)}$, $s_2=v_F$ are the charge- and spin-excitation velocities, respectively. For a general N, the velocities s_l are given by roots of the equation

$$\sum_{i=1}^{N}\frac{v_i}{s_l^2-v_i^2}=\frac{\pi\hbar}{V_0} \tag{A2}$$

and the coefficients γ_{il} are given by

$$\gamma_{il}^2=\frac{v_i}{(s_l^2-v_i^2)^2}\left[\sum_{j=1}^{N}\frac{v_j}{(s_l^2-v_j^2)^2}\right]^{-1}. \tag{A3}$$

In our system,[5] the Fermi velocities of the highest occupied bands are very different (e.g., the highest transverse mode has twice the velocity of the next lower-lying mode). Furthermore, since the interaction $V_0\lesssim\max(\hbar v_i)$ is not too large, the correction to the exponents α_i due to the interband coupling is expected to be relatively small. One can accommodate for this correction by slightly renormalizing the interaction constants g, viewing it as a mutual interband screening.[22]

Also, it is safe to disregard intermode transitions since they are determined by the Fourier components of the interaction with a large wave vector $k\sim k_F$, which are small for a smooth long-range potential.[22] The weak backscattering within each spin-degenerate mode can be further renormalized downward at low energies in the physical case of repulsive interactions.[15]

APPENDIX B: DIRECT TUNNELING FROM THE 2DEG

In order to describe the V and B dependencies of the conductance for direct 2DEG-lower-wire tunneling, we approximate the Green function of the top quantum well by the edge Green function of a 2D electron gas occupying a half plane $y>0$ with x extended from $-\infty$ to ∞. We assume the potential is $V(x,y)=0$ for $y>0$ and $V(x,y)=\infty$ for $y<0$. Therefore, we find

$$iG^{>}(x,y,t;x',y',0)=\frac{1}{\pi^2}\int_{-\infty}^{\infty}dp e^{ip(x-x')}\times\int_0^{\infty}dk\sin(ky)\sin(ky')\Theta(\epsilon)e^{-i\epsilon t/\hbar}, \tag{B1}$$

where $\epsilon=\hbar^2(p^2+k^2-k_F^2)/(2m)$ is the energy and k_F^2 is the Fermi wave vector of the 2DEG. $\Theta(\epsilon)$ is the Heaviside step function. When we calculate the tunneling current, y and y' run from 0 to ξ, the width of the tunnel junction (i.e., the extent of the 1D mode of the lower wire in the direction perpendicular to the cleaved edge). We set $(y,y')\to\xi/2$ and approximate $\sin(k\xi/2)\approx k\xi/2$ assuming $k_F<1/\xi$. In the frequency domain, the Green function $G^{>}(z,\omega)=\int_{-\infty}^{\infty}dt e^{i\omega t}G^{>}(z,t)$, with $z=x-x'$, then becomes

$$iG^{>}(z,\omega)=\frac{\xi^2}{2\pi\hbar}\int_{-\infty}^{\infty}dp e^{ipz}\int_0^{\infty}dk k^2\delta(\epsilon-\omega)\Theta(\omega). \tag{B2}$$

In the limit of small positive frequencies it reduces to

$$iG^{>}(z,\omega\to 0^+)=m\frac{\xi^2}{2\pi\hbar}\int_{-k_F}^{k_F}dp e^{ipz}\sqrt{k_F^2-p^2}=m(\xi k_F)^2\frac{J_1(k_F z)}{2\hbar k_F z}, \tag{B3}$$

where J_1 is the first-order Bessel function of the first kind. In particular, since $J_1(x)\propto x$ when $x\to 0$, the density of states is finite at the Fermi energy and $G^{>}(t)\propto 1/t$ as $t\to\infty$. Furthermore, from the low-energy form of the 2DEG Green function [Eq. (B3)] it follows that the relevant range of z in integral (9) is $1/k_F$ rather than $1/\max(q,\Gamma/v_F)$, as in the case of the 1D-1D tunneling.

[1] F.D.M. Haldane, J. Phys. C **14**, 2585 (1981), and references therein.

[2] J. Voit, Rep. Prog. Phys. **57**, 977 (1994).

[3] V. Meden and K. Schönhammer, Phys. Rev. B **46**, 15 753 (1992).

[4] J. Voit, Phys. Rev. B **47**, 6740 (1993).

[5] O.M. Auslaender, A. Yacoby, R. de Picciotto, K.W. Baldwin, L.N. Pfeiffer, and K.W. West, Science **295**, 825 (2002).

[6] D. Carpentier, C. Peça, and L. Balents, Phys. Rev. B **66**, 153304 (2002).

[7] U. Zülicke and M. Governale, Phys. Rev. B **65**, 205304 (2002).

[8] Y. Tserkovnyak, B.I. Halperin, O.M. Auslaender, and A. Yacoby, Phys. Rev. Lett. **89**, 136805 (2002).

[9] A. Yacoby, H.L. Stormer, K.W. Baldwin, L.N. Pfeiffer, and K.W. West, Solid State Commun. **101**, 77 (1997); L.N. Pfeiffer, A. Yacoby, H.L. Stormer, K.W. Baldwin, J. Hasen, A. Pinczuk, W. Wegscheider, and K.W. West, Microelectron. J. **28**, 817 (1997).

[10] A. Yacoby, H.L. Stormer, N.S. Wingreen, L.N. Pfeiffer, K.W. Baldwin, and K.W. West, Phys. Rev. Lett. **77**, 4612 (1996).
[11] D. Boese, M. Governale, A. Rosch, and U. Zülicke, Phys. Rev. B **64**, 085315 (2001).
[12] M. Bockrath, D.H. Cobden, J. Lu, A.G. Rinzler, R.E. Smalley, L. Balents, and P.L. McEuen, Nature (London) **397**, 598 (1999).
[13] R. de Picciotto, H.L. Stormer, A. Yacoby, L.N. Pfeiffer, K.W. Baldwin, and K.W. West, Phys. Rev. Lett. **85**, 1730 (2000).
[14] If we assume $\beta = L/l$ in Eq. (23), where l is a fixed length, then for large L, $U_u(x)$ takes the form which is independent of L at the boundaries: $U_u(x) \approx E_{\mathrm{Fu}} \exp[-2(L/2-|x|)/l]$. Note: α was used in Ref. 8 instead of β in Eq. (23); in this paper α denotes the LL exponent, see, e.g., Eq. (48).
[15] J. Sólyom, Adv. Phys. **28**, 201 (1979).
[16] S. Eggert, H. Johannesson, and A. Mattsson, Phys. Rev. Lett. **76**, 1505 (1996).
[17] T. Kawamura, H.A. Fertig, and J.P. Leburton, Phys. Rev. B **49**, R5105 (1994).
[18] A.E. Mattsson, S. Eggert, and H. Johannesson, Phys. Rev. B **56**, 15 615 (1997).
[19] M. Fabrizio and A.O. Gogolin, Phys. Rev. B **51**, 17 827 (1995).
[20] O.M. Auslaender, A. Yacoby, R. de Picciotto, K.W. Baldwin, L.N. Pfeiffer, and K.W. West, Phys. Rev. Lett. **84**, 1764 (2000).
[21] J. Rubio, J. M. Calleja, A. Pinczuk, B. S. Dennis, L. N. Pfeiffer, and K. W. West (unpublished).
[22] K.A. Matveev and L.I. Glazman, Phys. Rev. Lett. **70**, 990 (1993).